5912 *Inorg. Chem.* **2010**, *49*, 5912–5922
DOI: 10.1021/ic100377s

Inorganic Chemistry
Article

Structural Chemistry and Magnetic Properties of $Ln_{18}Li_8Rh_{5-x}Fe_xO_{39}$ (Ln = La, Nd)

Peter D. Battle,* Siân E. Dutton, and Nirawat Thammajak

Inorganic Chemistry Laboratory, Oxford University, South Parks Road, Oxford OX1 3QR, United Kingdom

Fernande Grandjean and Moulay T. Sougrati

Department of Physics, B5, University of Liège, B-4000 Sart-Tilman, Belgium

Gary J. Long*

Department of Chemistry, Missouri University of Science and Technology, University of Missouri, Rolla, Missouri 65409-0010

Katsuyoshi Oh-ishi and Shinji Nakanishi

Department of Applied Chemistry, Faculty of Science and Engineering, Chuo University, 1-13-27 Kasuga Bunkyo-ku, Tokyo 112-8551 Japan

Received February 24, 2010

Polycrystalline samples of $Ln_{18}Li_8Rh_{5-x}Fe_xO_{39}$ (Ln = La, Nd; $0.5 \leq x \leq 5$) have been synthesized by a solid-state method and studied by a combination of dc and ac magnetometry, neutron diffraction, and Mössbauer spectroscopy. All compositions adopt a cubic structure (space group $Pm\bar{3}n$, $a_0 \sim 12$ Å) based on intersecting ⟨111⟩ chains made up of alternating octahedral and trigonal-prismatic coordination sites. These chains occupy channels within a Ln−O framework. At low values of x, iron preferentially occupies the smaller (2*a*) of the two distinct octahedral sites as low-spin Fe(IV). The Rh(III) on the larger (8*e*) octahedral site is replaced by high-spin Fe(III). Nd-containing compositions having $x > 1$ show spin-glass-like behavior below ∼5 K. La-containing compositions having $x > 1$ show evidence of a magnetic transition at ∼8 K, but the nature of the transition is unclear. This contrasting behavior demonstrates that, although the structural chemistry of the two systems is essentially the same, the magnetic character of the Ln cations plays an important role in determining the properties of these compounds.

Introduction

$La_{18}Li_8Rh_5O_{39}$[1] adopts the crystal structure shown in Figure 1. Chains of coordination polyhedra, in which octahedral sites alternate with trigonal prismatic sites, occupy channels within a La−O framework. The chains and channels run along the ⟨111⟩ directions of the cubic unit cell, and the chains intersect each other at (0, 0, 0) and (1/2, 1/2, 1/2). Equivalent octahedral sites are located at these two points of intersection, and a further, crystallographically distinct octahedral site is located halfway between them. The two distinct types of octahedral site, both occupied by rhodium, are always separated from each other by a prismatic site which is occupied by lithium. The Rh^{3+} and Rh^{4+} cations, which occur in a 4:1 ratio in $La_{18}Li_8Rh_5O_{39}$, are found respectively on the 8*e* and 2*a* sites of space group $Pm\bar{3}n$; the midchain 8*e* site is significantly larger than the 2*a* site at the points of intersection, and the size difference is responsible for the cation ordering. The Li^+ cations are located on 16*i* sites within the prisms. We have shown in a series of publications[2−4] that the second-row transition-metal element in $Ln_{18}Li_8Rh_5O_{39}$ (Ln = La, Nd, Pr) can be replaced by several combinations of first-row elements to form $Ln_{18}Li_8M_{5-x}M'_xO_{39}$ (M, M′ = Mn, Fe, Co).

*To whom correspondence should be addressed. E-mail: peter.battle@chem.ox.ac.uk (P.D.B.); glong@mst.edu (G.J.L.).

(1) Frampton, P. P. C.; Battle, P. D.; Ritter, C. *Inorg. Chem.* **2005**, *44*, 7138.

(2) Dutton, S. E.; Battle, P. D.; Grandjean, F.; Long, G. J.; Oh-ishi, K. *Inorg. Chem.* **2008**, *47*, 11212.

(3) Dutton, S. E.; Battle, P. D.; Grandjean, F.; Long, G. J.; van Daesdonk, P. A. *Inorg. Chem.* **2009**, *48*, 1613.

(4) Dutton, S. E.; Battle, P. D.; Grandjean, F.; Long, G. J.; Sougrati, M. T.; van Daesdonk, P. A.; Winstone, E. *J. Solid State Chem.* **2009**, *182*, 1638.

Published on Web 06/09/2010

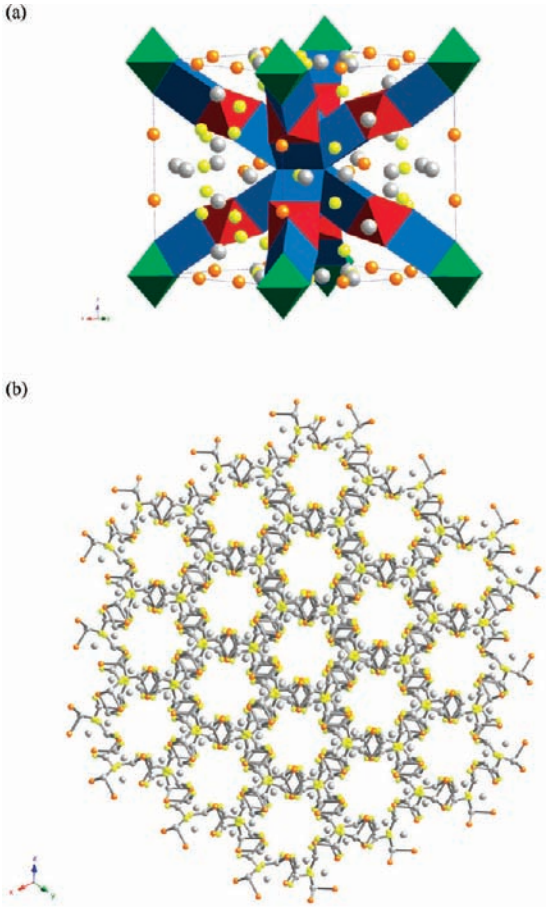

Figure 1. (a) Polyhedral representation of the structure of $La_{18}Li_8Rh_5O_{39}$. LiO_6 trigonal prisms are blue (16*i* site), RhO_6 octahedra are green (2*a*) and red (8*e*), gray circles represent oxygen (O2 and O3), yellow circles represent La1, and orange circles represent La2. (b) The La−O2−O3 framework viewed along ⟨111⟩. The polyhedral chains run through the channels.

However, apparently not all permutations of Ln, M, and M′ are allowed. We have ascribed this to the need to match the size of the ⟨111⟩ channels within the Ln−O framework to the size of the cations contained within the polyhedral chains. On the basis of the low-spin configurations adopted by iron(IV) on the 2*a* sites and manganese(III) on the 8*e* sites, we have proposed that the polyhedra are subjected to a significant chemical pressure, with the magnitude of the pressure being determined largely by the diameter of the channel in which they lie. It is reasonable to postulate that only a finite pressure range can be tolerated, and that the ratio of the ionic radii of the lanthanide element and the transition element must therefore be important in determining the stability of any given composition. In order to test this hypothesis, we have now synthesized and characterized compositions in the system $La_{18}Li_8Rh_{5-x}Fe_xO_{39}$; that is, we have systematically reduced the mean radius of the transition-metal cations while attempting to keep the channel size constant. We have also characterized compositions in the system $Nd_{18}Li_8Rh_{5-x}Fe_xO_{39}$, wherein the lanthanide radius is again held constant but at a lower value. We describe below the structural and magnetic characteristics of these compounds.

Experimental Section

Polycrystalline samples of $Ln_{18}Li_8Rh_{5-x}Fe_xO_{39}$ (Ln = La, Nd) were synthesized by grinding together stoichiometric quantities of oxide starting materials (lanthanum(III) oxide (99.99%, Alfa Aesar), neodymium(III) oxide (99.99%, Alfa Aesar), iron(III) oxide (99.998%, Alfa Aesar), and rhodium-(III) oxide (99.99%, Alfa Aesar)) and a 50% excess of volatile lithium carbonate (AnalaR) prior to firing in pellet form at 800 °C in the air for 12 h. A further 50% excess lithium carbonate was ground into the reaction mixture before it was fired again in the air for 1 h, as a pellet, at 1000 °C. X-ray powder diffraction was used to monitor the progress of the reactions. Further 1 h firings, with the addition of 50% excess lithium carbonate, were carried out on samples that X-ray powder diffraction showed to be impure at this stage.

All X-ray powder diffraction was carried out on a Philips X'pert diffractometer operating with Cu $K\alpha_1$ radiation with a step size of $\Delta 2\theta = 0.0084°$. High-intensity X-ray powder diffraction data were collected over a small angular range ($15 \leq 2\theta/° \leq 40$) in an attempt to detect lithium-containing impurities. High-resolution X-ray powder diffraction data for use in quantitative analysis were collected over the angular range $5 \leq 2\theta/° \leq 125$. Limited Rietveld[5] refinement of the structures was carried out using the GSAS[6] suite of programs. Backgrounds were fitted using a Chebyshev polynomial of the first kind, and the peak shape was modeled using a pseudo-Voigt function.

The diffractometers D2b and D1a at the Institut Laue Langevin, Grenoble, France were used to collect neutron powder diffraction data on selected samples using wavelengths of ∼1.59 and 1.91 Å, respectively. The unit-cell parameters derived from X-ray diffraction data were used to calibrate accurately the neutron wavelength. Data were collected over the angular range $5 \leq 2\theta/° \leq 160$ with a step size $\Delta 2\theta = 0.05°$ at room temperature and, in some cases, at 4.2 K. Samples (∼0.5 g) were contained within vanadium cans (ϕ = 5 mm) and, when a low-temperature measurement was to be carried out, mounted in a cryofurnace. Rietveld refinements of the structures were carried out using either the FULLPROF[7] or GSAS program. The background level was refined using the software. Peak shapes were modeled using a pseudo-Voigt function together with a correction for peak asymmetry.

Magnetic measurements were carried out using a Quantum Design MPMS 5000 SQUID magnetometer. The magnetization (M) was measured as a function of temperature on warming from 2 to 300 K after cooling both in a zero field (ZFC) and in the measuring field of 100 Oe (FC). The isothermal magnetization was measured as a function of the field ($-50 \leq H/kOe \leq 50$) after cooling to the measuring temperature at 50 kOe. The ac susceptibility data were recorded on selected samples at up to 11 frequencies ($0.5 \leq \omega/Hz \leq 1000$) in a dc field of ∼2 Oe and an oscillating field of amplitude 3.5 Oe over an appropriate temperature range with a temperature step size of 0.1 K.

The Mössbauer spectrum of $La_{18}Li_8Fe_5O_{39}$ has been measured between 4.2 and 295 K, and the spectra of $La_{18}Li_8Rh_{5-x}Fe_xO_{39}$, with $x = 1-4$, have all been measured at 295 K and for x = 4, 3.5, and 2.5 between 295 and 85, 25, or 85 K, respectively. The spectrum of $Nd_{18}Li_8Rh_3Fe_2O_{39}$ has been measured between 295 and 25 K. All the spectra were measured in a Janis Supervaritemp cryostat with a constant-acceleration spectrometer which utilized a rhodium matrix cobalt-57 source and was calibrated at room temperature with α-iron powder. The Mössbauer spectral absorbers contained 30−34 mg/cm^2 of the powder sample mixed with boron nitride. The ideal thickness of the Mössbauer absorber is limited to this rather small thickness because of the strong

(5) Rietveld, H. M. *J. Appl. Crystallogr.* **1969**, *2*, 65.
(6) Larson, A. C.; von-Dreele, R. B. *General Structure Analysis System* (*GSAS*); LAUR 86-748, Los Alamos National Laboratories: Los Alamos, NM, 1994.
(7) Rodriguez-Carvajal, J. *Physica B* **1993**, *192*, 55.

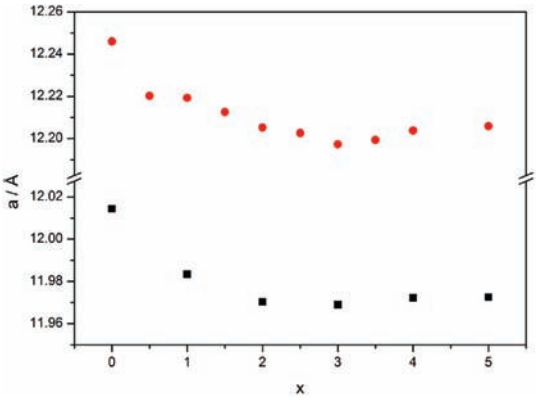

Figure 2. Composition dependence of the unit-cell parameter of $Ln_{18}Li_8Rh_{5-x}Fe_xO_{39}$ for Ln = La (●) and Nd (■), as determined by X-ray diffraction. The error bars are smaller than the size of the data points.

nonresonant scattering of the γ-rays by the 18 lanthanide ions per formula unit. This effect is, at least in part, responsible for the rather low signal-to-noise ratio observed in some of the lower temperature spectra. For the 2*a* and 8*e* sites, the relative statistical errors associated with the isomer shifts, quadrupole splittings, and line widths are ±0.005, ± 0.01, and ±0.01 mm/s, respectively; these errors are approximately twice as large for the 16*i* site. The absolute errors of these parameters are approximately twice the statistical errors.

Results

i. $La_{18}Li_8Rh_{5-x}Fe_xO_{39}$. X-ray powder diffraction data collected from compositions in the series $La_{18}Li_8Rh_{5-x}Fe_xO_{39}$ showed no evidence of impurity phases for $x < 3.0$; the more iron-rich samples contained a lithium carbonate impurity. The diffraction pattern of the target compound could always be indexed in the cubic space group $Pm\bar{3}n$. The composition dependence of the unit-cell parameter is shown in Figure 2; the dominance of the scattering by the heavy atoms prevented a full refinement of the crystal structure against the X-ray data.

Neutron diffraction data were collected from the compositions $x = 2.5$ and 3.5 at room temperature using the diffractometer D2b. The structure of $La_{18}Li_8Rh_5O_{39}$ was used as a starting point in the subsequent analysis. Note that the atom O4 is disordered and occupies the 48*l* site with a fractional occupancy of 0.25, rather than the 12*f* site. Refinement of the fractional occupancies of the two octahedral sites (2*a* and 8*e*) showed rhodium to be present on both octahedra in the $x = 2.5$ composition. However, preliminary analysis showed that the smaller 2*a* (0, 0, 0) site was fully occupied by iron in the composition $x = 3.5$, and in subsequent refinements, the occupation of this site was constrained accordingly. The atomic displacement factors for the 8*e* octahedral site and the 16*i* trigonal-prismatic site initially refined to unusually large values. The possibility of cation disorder between the two sites was therefore considered. A number of models in which either iron, rhodium, or both were allowed to occupy the trigonal-prism site were tested. These models involved either a concomitant transfer of lithium onto the vacant octahedral site or an overall lithium deficiency. For both compositions, $La_{18}Li_8Rh_{2.5}Fe_{2.5}O_{39}$ and $La_{18}Li_8Rh_{1.5}Fe_{3.5}O_{39}$, the best model was found to be that in which some iron was allowed to occupy the prismatic site

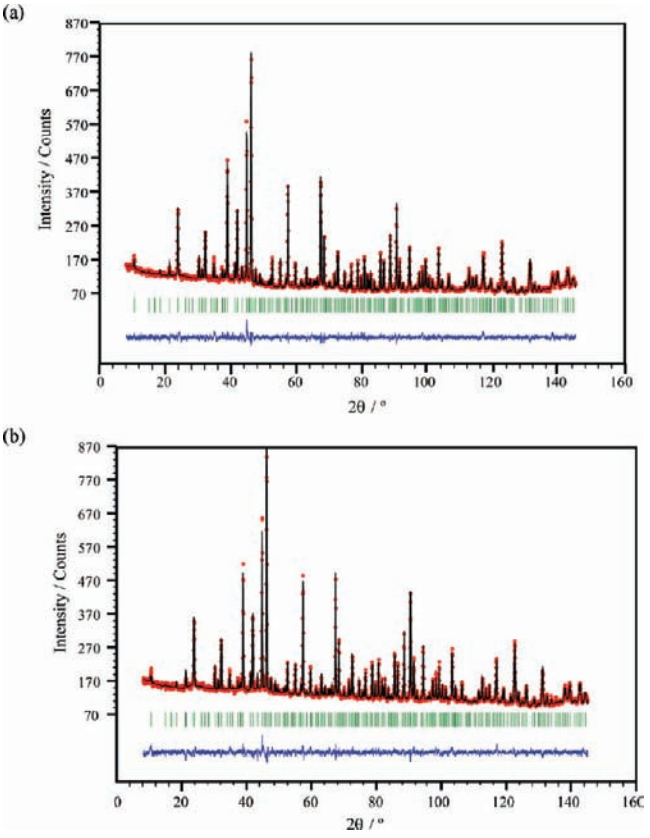

Figure 3. Observed and calculated neutron diffraction profiles of $La_{18}Li_8Rh_{5-x}Fe_xO_{39}$ for (a) $x = 2.5$ and (b) $x = 3.5$. A difference curve is also shown. Reflection positions are indicated by the vertical bars.

with lithium moving to the 8*e* octahedron at (1/4, 1/4, 1/4), thus maintaining the overall stoichiometry. In the composition $La_{18}Li_8Rh_{1.5}Fe_{3.5}O_{39}$, the concentration of iron on the trigonal-prism site was such that the resultant average neutron scattering factor for the site was very low. Consequently, the displacement factor for this site had to be constrained to be zero. The observed and calculated diffraction profiles of $La_{18}Li_8Rh_{2.5}Fe_{2.5}O_{39}$ and $La_{18}Li_8Rh_{1.5}Fe_{3.5}O_{39}$ are shown in Figure 3; structural parameters and selected bond lengths and angles are given in Tables 1 and 2, respectively.

D2b was also used to collect neutron diffraction data on $La_{18}Li_8Fe_5O_{39}$, at room temperature and 4.2 K. No additional Bragg scattering was observed in the data collected at 4.2 K, and it was therefore assumed that this compound does not show long-range magnetic order at and above 4.2 K. Both data sets could be analyzed using a model in which the 2*a* site is occupied exclusively by iron. The majority of the remaining iron occupies the 8*e* sites, although there is some site exchange with lithium from the 16*i* sites. The synthesis of this sample was more challenging than those of the compositions $x < 5$ and necessitated the use of a significant excess of lithium carbonate. The unreacted carbonate was included as a second phase in the analysis of the neutron diffraction data. The refined structural parameters of the principal phase are listed in Table 3, and the most important bond lengths are given in Table 4. The fit to the data collected at 4.2 K is shown in Figure S1 (Supporting Information); a region of the profile at $2\theta \sim 125°$ had to be excluded from the refinement

Table 1. Structural Parameters of $La_{18}Li_8Rh_{2.5}Fe_{2.5}O_{39}$ and $La_{18}Li_8Rh_{1.5}Fe_{3.5}O_{39}$ at Room Temperature

		$La_{18}Li_8Rh_{2.5}$-$Fe_{2.5}O_{39}$	$La_{18}Li_8Rh_{1.5}$-$Fe_{3.5}O_{39}$
a/Å		12.2026(1)	12.1993(1)
R_{wp}		0.049	0.059
χ^2		1.88	2.26
La1 24*k*	*y*	0.3073(3)	0.3076(3)
0 *y z*	*z*	0.3040(3)	0.3041(3)
	U_{iso}/Å^2	0.0144(5)	0.0142(5)
La2 12*f*	*x*	0.3471(2)	0.3474(3)
(*x*, 0, 0)	U_{iso}/Å^2	0.0089(8)	0.0077(8)
Rh1(Fe) 2*a*	U_{iso}/Å^2	0.005(2)	0.009(2)
(0, 0, 0)	Rh occupancy	0.26(6)	0.0
	Fe occupancy	0.74(6)	1.0
Rh2(Fe/Li) 8*e*	U_{iso}/Å^2	0.023(2)	0.034(2)
(1/4, 1/4, 1/4)	Rh occupancy	0.56(2)	0.38
	Fe occupancy	0.31(2)	0.47(1)
	Li occupancy	0.13(1)	0.15(1)
Li1(Fe) 16*i*	*x*	0.3661(9)	0.3642(8)
(*x*, *x*, *x*)	U_{iso}/Å^2	0.011(5)	0.0
	Li occupancy	0.932 (10)	0.927(10)
	Fe occupancy	0.068(10)	0.073(10)
O1 48*l*	*x*	0.8636(3)	0.8635(3)
(*x*, *y*, *z*)	*y*	0.8610(3)	0.8607(3)
	z	0.6951(2)	0.6953(2)
	U_{iso}/Å^2	0.0132(5)	0.0122(5)
O2 6*d*	U_{iso}/Å^2	0.014(1)	0.011(2)
(1/4, 1/2, 0)			
O3 12*g*	*x*	0.6316(5)	0.6330(5)
(*x*, 0)	U_{iso}/Å^2	0.009(1)	0.009(1)
O4 48*l*	*x*	0.1550(7)	0.1523(8)
(*x*, *y*, *z*)	*y*	0.016(3)	0.020(2)
	z	−0.021(2)	−0.018(2)
	U_{iso}/Å^2	0.042(4)	0.043(5)
	occupancy	1/4	1/4

Table 2. Bond Lengths (Å) and Bond Angles (deg) in $La_{18}Li_8Rh_{2.5}Fe_{2.5}O_{39}$ and $La_{18}Li_8Rh_{1.5}Fe_{3.5}O_{39}$ at Room Temperature

	$La_{18}Li_8Rh_{2.5}Fe_{2.5}O_{39}$	$La_{18}Li_8Rh_{1.5}Fe_{3.5}O_{39}$
La1−O1	2.657(4) ×2	2.643(5) ×2
	2.574(4) ×2	2.573(4) ×2
	2.643(5) ×2	2.659(4) ×2
La1−O2	2.491(4)	2.491(4)
La1−O3	2.479(4)	2.469(4)
	3.154(4)	3.141(4)
La2−O1	2.392(3) ×4	2.436(3) ×4
La2−O3	2.432(3) ×2	2.469(5) ×2
La2−O4	2.413(9)	2.403(10)
Rh1(Fe)−O4	1.87(2) ×6	1.90 (2) ×6
Rh2(Fe/Li)−O1	2.050(3) ×6	2.046(3) ×6
Li1(Fe)−O1	2.087(12) ×3	2.061(10) ×3
Li1(Fe)−O4	2.332(3)[a] ×3	2.346(2)[a] ×3
Li1(Fe)−Li1(Fe)	3.267(16)	3.313(14)
Rh1(Fe)−Li1	2.829(11)	2.844(10)
Rh2(Fe/Li)−Li1	2.453(11)	2.413(10)
La1−La1 (pore size)	6.397(2)	6.397(2)
O1−Rh2(Fe/Li)−O1	89.4(2)	89.4(2)
	89.7(2)	89.5(2)
	91.4(2)	91.6(2)

[a] The average bond length to a disordered oxygen site.

because of the presence of a peak attributable to the cryofour.

The temperature dependence of the dc magnetic susceptibility of selected compositions in the series $La_{18}Li_8Rh_{5-x}Fe_xO_{39}$ is shown in Figure 4, and the parameters obtained by fitting the data collected at temperatures above 150 K to a Curie−Weiss law are listed in Table 5. The susceptibility of $La_{18}Li_8Rh_{4.5}Fe_{0.5}O_{39}$ increases smoothly on cooling, but, as can be seen in Figure 4b and c,

Table 3. Structural Parameters of $La_{18}Li_8Fe_5O_{39}$ at Room Temperature and 4.2 K

		room temperature	4.2 K
a/Å		12.20585(5)	12.1790(2)
R_{wp},		0.043	0.039
χ^2		3.1	3.0
La1 24*k*	*y*	0.3070(3)	0.3067(3)
(0, *y*, *z*)	*z*	0.3041(3)	0.3039(3)
	U_{iso}/ Å^2	0.0071(5)	0.0045(5)
La2 12*f*	*x*	0.3473(3)	0.3476(3)
(*x*, 0, 0)	U_{iso}/ Å^2	0.0014(8)	0.0000(8)
Fe1 2*a*	U_{iso}/ Å^2	0.007(2)	0.004(2)
(0, 0, 0)			
Fe2(Li) 8*e*	U_{iso}/ Å^2	0.017(1)	0.015(1)
(1/4, 1/4, 1/4)	Fe occupancy	0.86(1)	0.84(1)
	Li occupancy	0.14(1)	0.16(1)
Li1(Fe) 16*i*	*x*	0.367(1)	0.3664(9)
(*x*, *x*, *x*)	U_{iso}/ Å^2	0.005(6)	−0.005(5)
	Li occupancy	0.929(6)	0.922(6)
	Fe occupancy	0.071(6)	0.078(6)
O1 48*l*	*x*	0.8645(3)	0.8639(3)
(*x*, *y*, *z*)	*y*	0.8589(3)	0.8593(3)
	z	0.6950(2)	0.6949(2)
	U_{iso}/ Å^2	0.0075(5)	0.0059(5)
O2 6*d*	U_{iso}/ Å^2	0.008(2)	0.005(2)
(1/4, 1/2, 0)			
O3 12*g*	*x*	0.6312(5)	0.6313(5)
(*x*, 0, 1/2)	U_{iso}/ Å^2	0.005(1)	0.002(1)
O4 48*l*	*x*	0.1477(9)	0.1491(9)
(*x*, *y*, *z*)	*y*	0.020(2)	0.018(2)
	z	0.019(2)	0.019(2)
	U_{iso}/ Å^2	0.034(4)	0.027(4)
	occupancy	1/4	1/4

Table 4. Bond Lengths (Å) and Bond Angles (deg) in $La_{18}Li_8Fe_5O_{39}$ at Room Temperature and 4.2 K

bond/angles	room temperature	4.2 K
La1−O1	2.683(6) ×2	2.667(6) ×2
	2.614(6) ×2	2.614(6) ×2
	2.571(3) ×2	2.565(3) ×2
La1−O2	2.490(4)	2.486(5)
La1−O3	2.485(4)	2.483(4)
	3.163(6)	3.156(7)
La2−O1	2.443(3) ×4	2.440(3) ×4
La2−O3	2.458(5) ×2	2.450(5) ×2
La2−O4	2.46(1)	2.44(1)
Fe1−O4	1.83(1) ×6	1.84(1) ×6
Fe2(Li)−O1	2.043(3) ×6	2.036(3) ×6
Li1(Fe)−O1	2.10(1) ×3	2.09(1) ×3
Li1(Fe)−O4	2.32(5)[a] ×3	2.32(5)[a] ×3
Li1(Fe)−Li1(Fe)	3.25(3)	3.25(2)
Fe1−Li1	2.82(2)	2.82(2)
Fe2(Li)−Li1	2.47(2)	2.46(2)
La1−La1 (pore size)	6.397(1)	6.381(1)
O1−Fe2(Li)−O1	88.5(2)	88.8(2)
	89.6(1)	89.7(1)
	92.3(2)	91.9(2)

[a] The average bond length to a disordered oxygen site.

as the concentration of iron increases, an increasing level of hysteresis becomes apparent below ∼8 K. Although the gradient of $\chi(T)$ remains negative throughout the measured temperature range, there is a marked change in slope at this temperature. The field dependence of the magnetization at 300, 15, and 5 K is shown for $x = 5$ in Figure S2 (Supporting Information); nonlinearity is only apparent at 5 K. In an attempt to understand the origin of this behavior, the ac susceptibility of $La_{18}Li_8Fe_5O_{39}$ was measured in the low-temperature region. The results are shown in Figure 5.

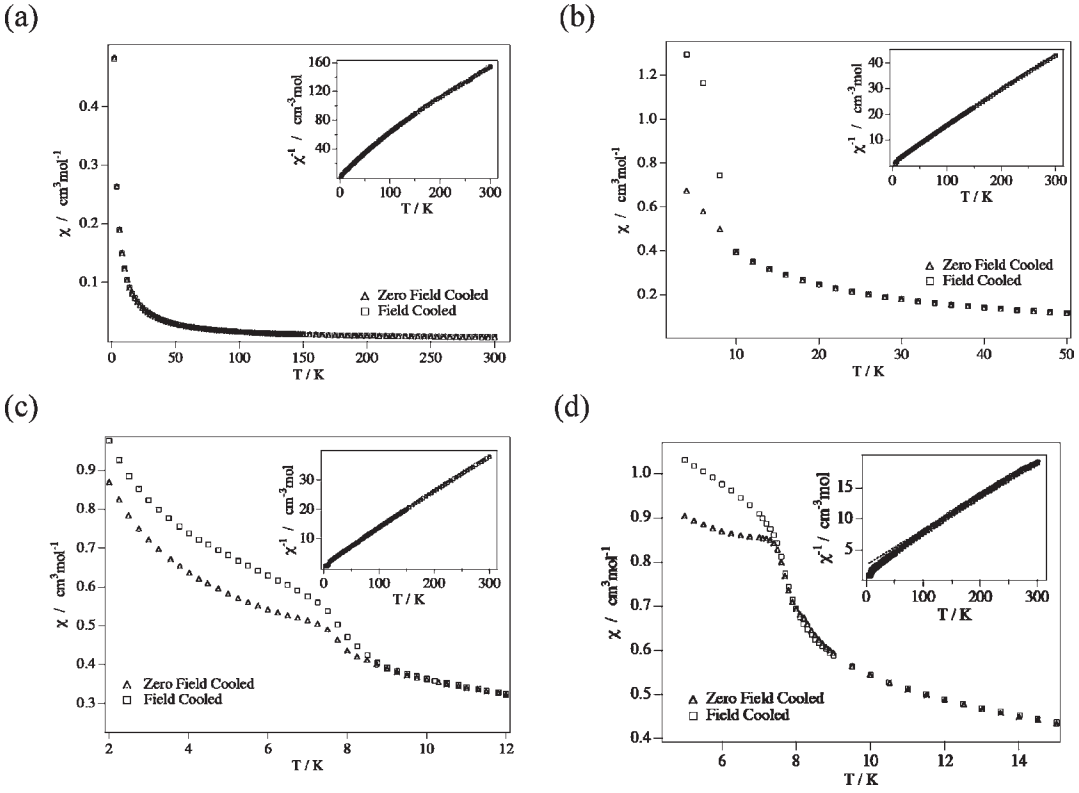

Figure 4. Temperature dependence of the dc molar magnetic susceptibility of $La_{18}Li_8Rh_{5-x}Fe_xO_{39}$ for x = (a) 0.5, (b) 2.0, (c) 3.5, and (d) 5.0.

Table 5. Curie–Weiss Parameters for $La_{18}Li_8Rh_{5-x}Fe_xO_{39}$

x	C_m/cm³ K mol^{-1}	θ/K	C_{calc}[a]/cm³ K mol^{-1} (Fe^{4+} LS)
0.5	2.29(1)	−56.1(1)	2.2
1.0	3.70(1)	−46.4(1)	4.0
1.5	6.03(2)	−32.2(8)	5.8
2.0	7.39(1)	−19.5(4)	7.6
2.5	8.45(3)	−24.2(7)	8.6
3.0	9.08(1)	−13.1(2)	9.8
3.5	8.36(2)	−19.5(4)	11.9
4.0	14.96(2)	−23.3(3)	14.1
5.0	17.29(6)	−37.8(7)	18.5

[a] For samples with $x < 2.5$, a random Rh/Fe distribution has been assumed. For $x = 2.5$ and $x = 3.5$, the Rh/Fe distribution determined by neutron diffraction has been used. For $x = 3.0$ and $x = 4.0$, the 2a site has been assumed to be fully occupied by Fe(IV). Calculations were made using the spin-only formula.

The Mössbauer spectra of $La_{18}Li_8Fe_5O_{39}$ have been measured between 4.2 and 295 K. Those obtained between 25 and 295 K were fit with one line width and three symmetric quadrupole doublets whose relative areas have been constrained to the iron occupancies of the 2a, 8e, and 16i sites as determined from the 4.2 K neutron diffraction refinements given in Table 3. The constrained percentage areas used for each site are given in Table S1 (Supporting Information), and the corresponding hyperfine parameters are given in Table S2 (Supporting Information). The results for selected spectra are shown in Figure 6, and the temperature dependencies of the resulting hyperfine parameters are shown in Figure 7.

The spectra of $La_{18}Li_8Fe_5O_{39}$ obtained at 4.2, 6, and 8 K show the onset of magnetic correlations or spin-freezing as is reflected in the dramatic increase in the width of the spectral profile and the appearance of a very

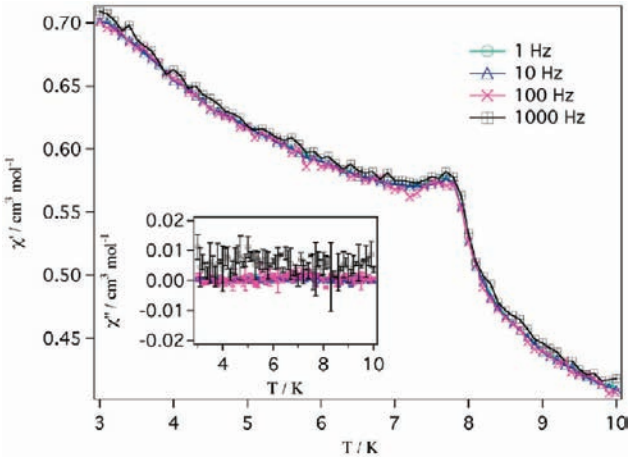

Figure 5. Temperature dependence of the ac molar magnetic susceptibility of $La_{18}Li_8Fe_5O_{39}$.

weak absorption at ca. −1 mm/s, an absorption that is just apparent at 8 K. In order to include this contribution in the spectral fits, an additional magnetic component, in black, has been added to the 4.2, 6, and 8 K fits, see Figure 6. Because of the broadened and unresolved nature of the magnetic component, in order to obtain these fits, the hyperfine parameters of the paramagnetic 2a, 8e, and 16i site components were constrained to be the same as observed at 25 K. Surprisingly, it was not possible to include a magnetic component with the same isomer shift, δ, and quadrupole splitting, ΔE_Q, as observed for the 8e site. However, satisfactory fits could be obtained by using the 25 K weighted average δ and the negative weighted average ΔE_Q. The resulting areas of the magnetic

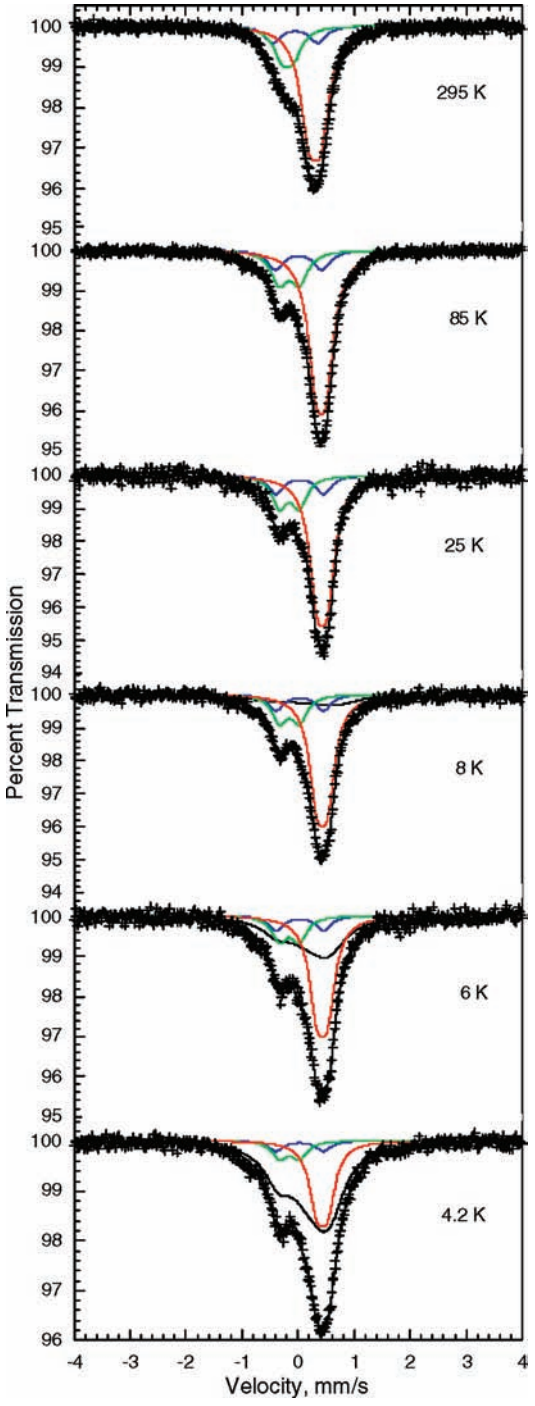

Figure 6. Selected Mössbauer spectra of $La_{18}Li_8Fe_5O_{39}$ obtained at the indicated temperatures and fit with three component quadrupole doublets corresponding to the 2*a* site, green; the 8*e* site, red; and the 16*i* site, blue. A magnetic component (black) is included at 8 K and below.

components are 62(2), 37(3), and 16(4)%, and the corresponding hyperfine fields are 2.6(2), 2.7(4), and 3(1) T at 4.2, 6, and 8 K, respectively. The hyperfine fields are highly correlated with the fitted magnetic component line widths of 0.66(6), 0.7(1), and 0.8(2) mm/s.

The observed isomer shifts of $La_{18}Li_8Fe_5O_{39}$, see the top of Figure 7, indicate that the 2*a*, 8*e*, and 16*i* sites are occupied by low-spin iron(IV), high-spin iron(III), and high-spin iron(III), respectively. The temperature dependencies of the isomer shifts of the 2*a*, 8*e*, and 16*i*

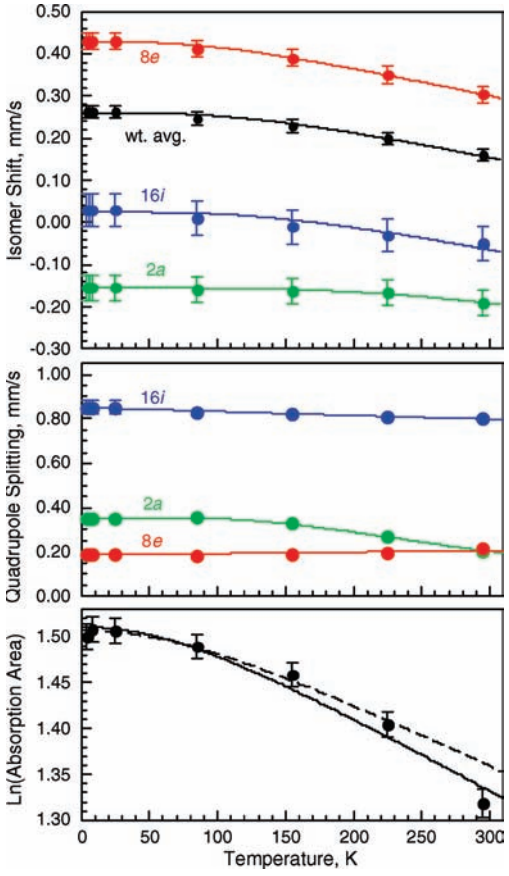

Figure 7. Temperature dependence of the $La_{18}Li_8Fe_5O_{39}$ Mössbauer spectral isomer shifts, top; quadrupole splittings, center; and the logarithm of the spectral absorption area, bottom. The fits of the isomer shifts of the 2*a* and 8*e* sites and the logarithm of the spectral absorption area correspond to fits with the Debye model for a solid. The line through the quadrupole splitting of the 2a site corresponds to a fit with the Ingalls model.

sites, and their weighted average, see the top of Figure 7, are well fit with the Debye model[8] for the second-order Doppler shift; the resulting Mössbauer temperatures, Θ_M, are 1270(64), 402(19), 653(79), and 535(30) K, respectively. The values for the 8*e* and 16*i* sites are reasonable for an iron(III) site and for the structure of $La_{18}Li_8Fe_5O_{39}$. However, the 1270(64) K value for the 2*a* site is much larger than expected for a low-spin iron(IV) ion.

The temperature dependence of the quadrupole splitting, ΔE_Q, of the 2*a* site in $La_{18}Li_8Fe_5O_{39}$ has been fit with the Ingalls[9] model that accounts for any changes in the q_{val} contribution to ΔE_Q with temperature, changes that would arise from variations in the thermal occupancy of the three t_{2g} d orbitals of the low-spin iron(IV) cation. The fit shown in the center of Figure 7 corresponds to a splitting of these three orbitals by 416(10) cm^{-1}. Because high-spin iron(III) has a $3d^5\ ^6A_{1g}$ electronic configuration, there is no q_{val} contribution to its ΔE_Q, which is composed solely of a virtually temperature independent q_{lat} contribution, a contribution that yields a temperature

(8) Shenoy, G. K.; Wagner, F. E.; Kalvius, G. M. In *Mössbauer Isomer Shifts*; Shenoy, G. K., Wagner, F. E., Eds.; North-Holland: Amsterdam, 1978; p 49.
(9) Ingalls, R. *Phys . Rev.* **1964**, *133A*, 787.

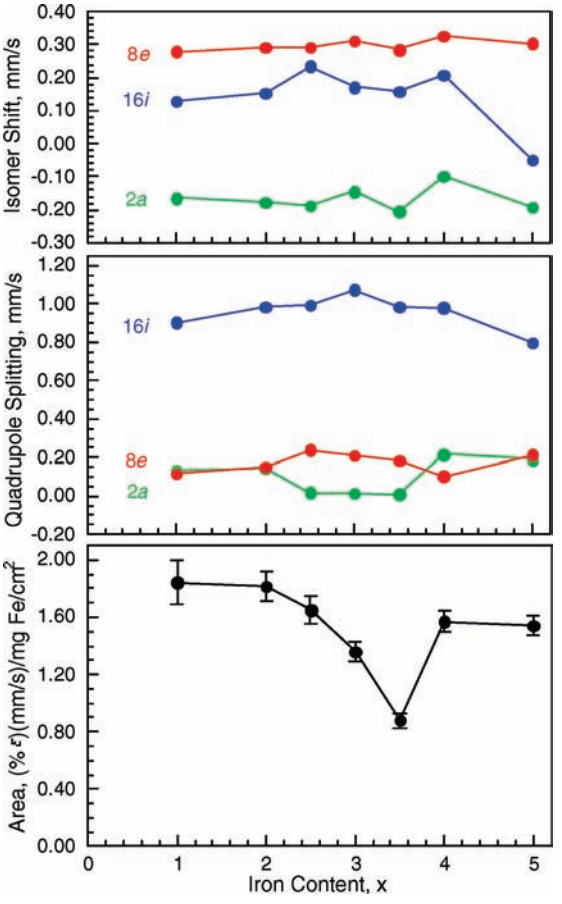

Figure 8. The 295 K compositional dependence of the $La_{18}Li_8Rh_{5-x}Fe_xO_{39}$ isomer shifts, top; quadrupole splittings, center; and the spectral mass-normalized absorption areas, bottom.

independent ΔE_Q for the high-spin iron(III) on the 8*e* and 16*i* sites.

The temperature dependence of the Mössbauer spectral absorption area of $La_{18}Li_8Fe_5O_{39}$ may also be fit with the Debye model[8] for a solid, see the bottom of Figure 7, and yields Debye temperatures, Θ_D, of 403(13) K for a fit between 8 and 295 K and 438(12) K for a fit between 8 and 225 K, values that are, as expected, somewhat smaller than the Θ_M value of 535(30) K obtained from the weighted average isomer shifts.

The 295 K Mössbauer spectra of $La_{18}Li_8Rh_{5-x}Fe_xO_{39}$ for $x = 1-4$ have also been measured and for $x = 4$, 3.5, and 2.5; the spectra of these compounds have been measured as a function of temperature between 295 and 85, 25, or 85 K, respectively. All of these spectra, except for $x = 1$, 2, and 2.5, have been fit with one line width and three symmetric quadrupole doublets whose relative areas have been constrained to the iron occupancies of the 2*a*, 8*e*, and 16*i* sites, as determined, see Figure S3 (Supporting Information), either from the neutron diffraction occupancies or by interpolation and extrapolation from the occupancies reported above for $x = 2.5$, 3.5, and 5. The constrained percentage areas used for each site and each compound are given in Table S1 (Supporting Information), and the corresponding hyperfine parameters are given in Table S2 (Supporting Information). The spectra obtained at 295 K for each compound are shown in Figure S4 (Supporting Information), and the compositional dependencies of the resulting

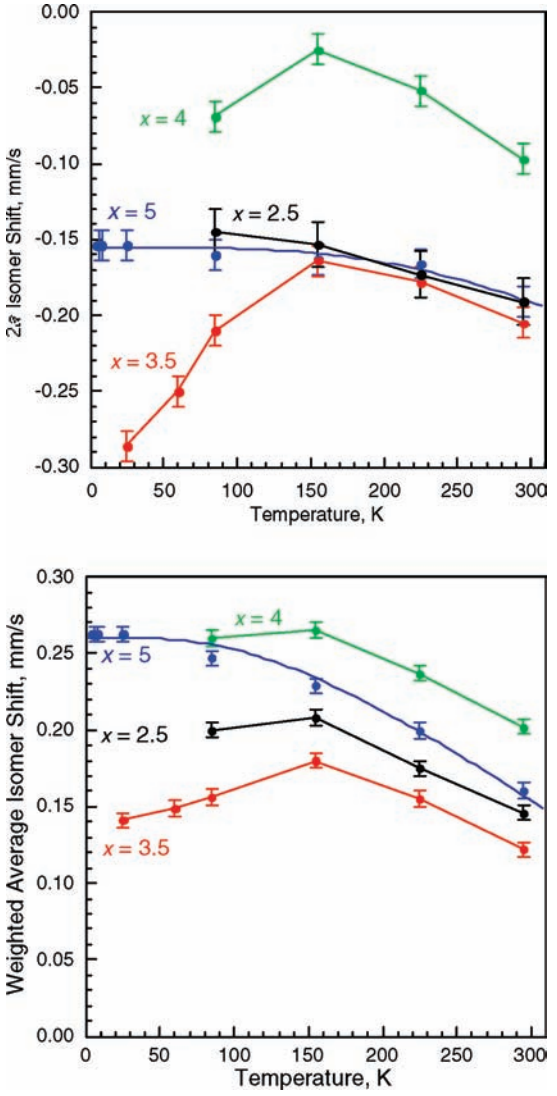

Figure 9. Temperature dependence of the 2*a* site isomer shift, top, and the weighted average isomer shift, bottom, of $La_{18}Li_8Rh_{5-x}Fe_xO_{39}$ for the indicated *x* values.

hyperfine parameters are shown in Figure 8. Selected spectra obtained between 25 and 295 K for $La_{18}Li_8Rh_{5-x}Fe_xO_{39}$ with $x = 2.5$ and 3.5 are shown in Figures S5 and S6 (Supporting Information), and a comparison of the temperature dependence of the iron(IV) 2*a* site isomer shift and the weighted average of all the isomer shifts of $La_{18}Li_8Rh_{5-x}Fe_xO_{39}$ is shown in Figure 9. We note in particular that the spectrum of $La_{18}Li_8Rh_{1.5}Fe_{3.5}O_{39}$ collected at 25 K could be fitted without the use of a hyperfine field.

ii. $Nd_{18}Li_8Rh_{5-x}Fe_xO_{39}$. The limiting compositions of this series, $x = 0$ and 5, have been prepared previously.[2,10] X-ray powder-diffraction data collected on samples prepared in the present study showed that isostructural single phase samples of $Nd_{18}Li_8Rh_{5-x}Fe_xO_{39}$ can also be obtained for $1 \leq x \leq 4$. The unit cell parameters of these compositions are plotted in Figure 2.

Neutron diffraction data were collected from the compositions $x = 1$ and 2 at room temperature using the diffractometer D1a. In $x = 1$, the 2*a* site was found to be

(10) Frampton, P. P. C. D. Phil. Thesis; University of Oxford, Oxford, U. K., 2005.

Table 6. Structural Parameters of $Nd_{18}Li_8Rh_4FeO_{39}$ and $Nd_{18}Li_8Rh_3Fe_2O_{39}$ at Room Temperature

		$Nd_{18}Li_8Rh_4FeO_{39}$	$Nd_{18}Li_8Rh_3Fe_2O_{39}$
a/Å		11.9805(3)	11.9744(3)
R_{wp}		0.032	0.028
χ^2		2.97	2.10
Nd1 24*k*	*y*	0.3082(2)	0.3077(2)
(0, *y*, *z*)	*z*	0.3056(2)	0.3062(2)
	U_{iso}/Å^2	0.0074(5)	0.0060(4)
Nd2 12*f*	*x*	0.3465(2)	0.3469(2)
(*x*, 0, 0)	U_{iso}/Å^2	0.0027(7)	0.0023(6)
Rh1(Fe) 2*a*	U_{iso}/Å^2	−0.001(2)	0.008(1)
(0, 0, 0)	Rh occupancy	0.42(4)	0.00
	Fe occupancy	0.58(4)	1.00
Rh2(Fe/Li) 8*e*	U_{iso}/Å^2	0.011(1)	0.0059(9)
(1/4, 1/4, 1/4)	Rh occupancy	0.894(9)	0.75
	Fe occupancy	0.070(8)	0.16
	Li occupancy	0.036(6)	0.09
Li1(Fe) 16*i*	*x*	0.3743(5)	0.3739(6)
(*x*, *x*, *x*)	U_{iso}/Å^2	0.001(3)	0.00
	Li occupancy	0.982(3)	0.955
	Fe occupancy	0.018(3)	0.045
O1 48*l*	*x*	0.8650(2)	0.8655(2)
(*x*, *y*, *z*)	*y*	0.8612(2)	0.8608(2)
	z	0.6922(2)	0.6926(2)
	U_{iso}/Å^2	0.0108(5)	0.0100(4)
O2 6*d*	U_{iso}/Å^2	0.015(2)	0.017(1)
(1/4, 1/2, 0)			
O3 12*g*	*x*	0.6308(3)	0.6297(3)
(*x*, 0)	U_{iso}/Å^2	0.005(1)	0.004(1)
O4 48*l*	*x*	0.1529(4)	0.1526(4)
(*x*, *y*, *z*)	*y*	0.018(1)	0.016(1)
	z	0.018(1)	0.0208(9)
	U_{iso}/Å^2	0.013(3)	0.013(3)
	occupancy	1/4	1/4

occupied by both rhodium and iron in a disordered manner. However, when the iron concentration is increased to $x = 2$, the Mössbauer spectral data, see below, show that the 2*a* site is occupied only by iron. In both cases, the 8*e* site is occupied principally by rhodium and iron, although there is again some site exchange between iron and lithium from the trigonal-prismatic 16*i* site. The observed and calculated neutron diffraction profiles of these two compositions are shown in Figure S7 (Supporting Information); the refined structural parameters and selected bond lengths are given in Tables 6 and 7, respectively.

The temperature dependence of the dc molar magnetic susceptibility of selected compositions in the series $Nd_{18}Li_8Rh_{5-x}Fe_xO_{39}$ is shown in Figure 10, and the parameters derived by fitting the data collected above 150 K to a Curie−Weiss law are listed in Table 8. In view of the hysteresis apparent at low temperatures, the ac susceptibility of the composition $x = 2$ was also measured; the results are shown in Figure 11. The parameter $\kappa = \Delta T_f/T_f \Delta \log \omega$ takes a value of 0.045, which is characteristic of an insulating spin glass.[11]

The iron-57 Mössbauer spectra of $Nd_{18}Li_8Rh_3Fe_2O_{39}$ have been measured between 25 and 295 K, and selected spectra are shown in Figure 12. The spectra indicate that $Nd_{18}Li_8Rh_3Fe_2O_{39}$ is paramagnetic between 60 and 295 K and just begins to exhibit weak magnetic correlations at 25 K. The temperature dependence of the spectral parameters is shown in Figure 13.

(11) Mydosh, J. A. *Spin Glasses: An Experimental Introduction*; Taylor & Francis: London, 1993.

Table 7. Bond Lengths (Å) and Bond Angles (deg) in $Nd_{18}Li_8Rh_4FeO_{39}$ and $Nd_{18}Li_8Rh_3Fe_2O_{39}$ at Room Temperature

	$Nd_{18}Li_8Rh_4FeO_{39}$	$Nd_{18}Li_8Rh_3Fe_2O_{39}$
Nd1−O1	2.635(4) ×2	2.647(4) ×2
	2.595(4) ×2	2.582(4) ×2
	2.492(2) ×2	2.496(2) ×2
Nd1−O2	2.431(2)	2.422(2)
Nd1−O3	2.421(3)	2.427(2)
	3.110(4)	3.125(4)
Nd2−O1	2.365(2) ×4	2.365(2) ×4
Nd2−O3	2.416(3) ×2	2.403(3) ×2
Nd2−O4	2.340(5)	2.348(5)
Rh1(Fe)−O4	1.858(5) ×6	1.854(5) ×6
Rh2(Fe/Li)−O1	2.038(2) ×6	2.036(2) ×6
Li1(Fe)−O1	2.190(7) ×3	2.178(8) ×3
Li1(Fe)−O4	2.17(3)[a] ×3	2.17(3)[a] ×3
Li1(Fe)−Li1(Fe)	3.01(1)	3.02(1)
Rh1(Fe)−Li1	2.61(1)	2.62(1)
Rh2(Fe/Li)−Li1	2.58(1)	2.57(1)
Nd1−Nd1 (pore size)	6.2932(8)	6.2902(7)
O1−Rh2(Fe/Li)−O1	88.2(1)	88.1(1)
	90.6(7)	90.37(7)
	90.7(1)	91.2(1)

[a] The average bond length to a disordered oxygen site.

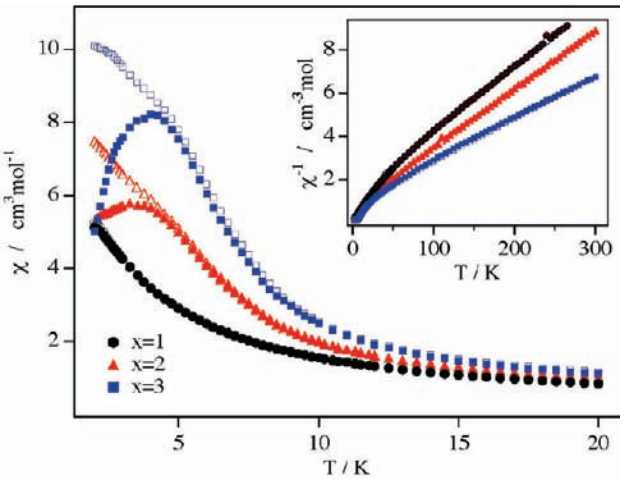

Figure 10. Temperature dependence of the dc molar magnetic susceptibility of $Nd_{18}Li_8Rh_{5-x}Fe_xO_{39}$.

Table 8. Curie−Weiss Parameters for $Nd_{18}Li_8Rh_{5-x}Fe_xO_{39}$

x	C_m/cm^3 K mol^{-1}	θ/K	C_{calc}/cm^3 K mol^{-1}[a]
1.0	34.0(1)	−46.1(8)	32.0
2.0	37.01(6)	−29.5(3)	34.8
3.0	52.0(3)	−52.8(2)	39.2

[a] Calculated using the spin-only formula for Fe and Rh, assuming Fe(IV) and Rh(IV) are low spin and Fe(III) is high spin; the 2*a* site was assumed to be occupied only by Fe for $x \geq 2$.

The paramagnetic spectra obtained at 60 K and above have been fit with three doublets assigned to the 2*a*, 8*e*, and 16*i* sites; the relative areas of these sites refined to be 50, 32 and 18%, respectively, and these values were used to define the iron occupancy of the sites in the analysis of the neutron diffraction data collected at room temperature, see Table 6. The spectrum obtained at 25 K is broadened relative to the 60 K spectrum, and as a consequence, it has been fit with one paramagnetic doublet and one small hyperfine field sextet for the 2*a* site and with doublets for both the 8*e* and 16*i* sites. The relative areas for the three

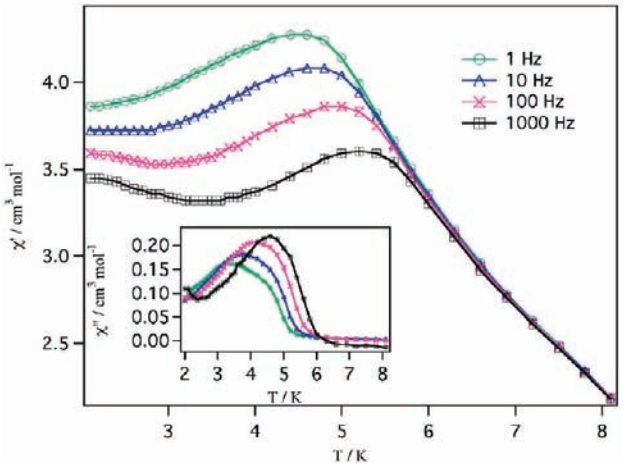

Figure 11. Temperature dependence of the ac molar magnetic susceptibility of $Nd_{18}Li_8Rh_3Fe_2O_{39}$.

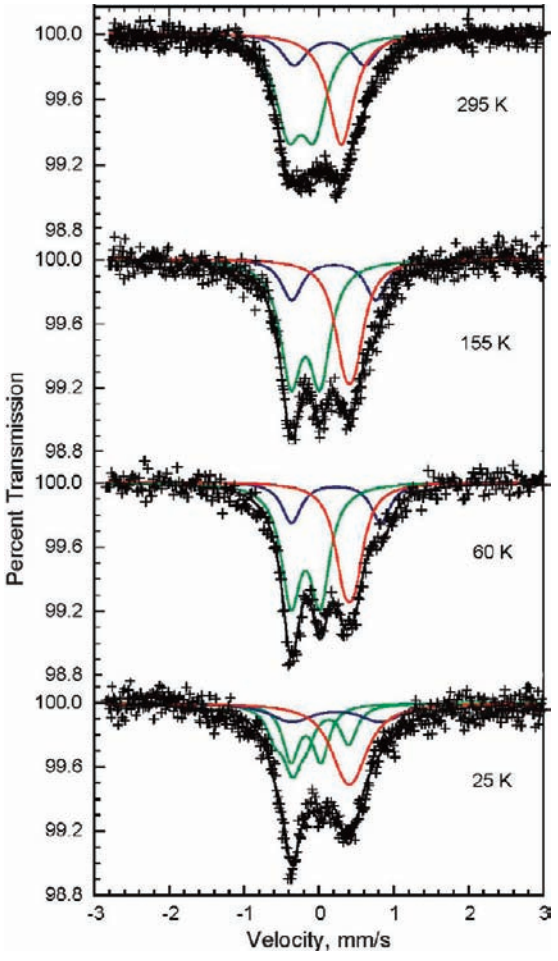

Figure 12. Iron-57 Mössbauer spectra of $Nd_{18}Li_8Rh_3Fe_2O_{39}$ measured at the indicated temperatures. The green, red, and blue lines correspond to the components assigned to the 2*a*, 8*e*, and 16*i* sites, respectively.

sites have been constrained to be in the same ratio as at the higher temperatures. Both the isomer shift and quadrupole splitting for the paramagnetic quadrupole doublet and the magnetic sextet have been constrained to be the same. The resulting best fit indicated that the two 2*a* site components have relative areas of 21(2) and 29(2) %,

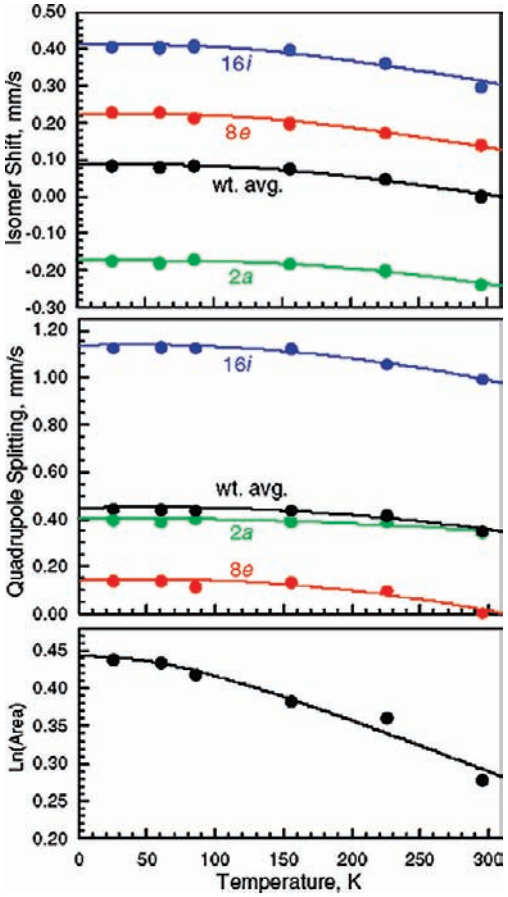

Figure 13. Temperature dependence of the Mössbauer spectral isomer shifts, top, and quadrupole splittings, center, for the 2*a*, 8*e*, and 16*i* sites, and their weighted average, and the logarithm of the spectral absorption area of $Nd_{18}Li_8Rh_3Fe_2O_{39}$. The errors for the 2*a* and 8*e* sites and the weighted average are at most the size of the data points and for the 16*i* site are at most twice the size of the data points. The isomer shifts and absorption area have been fit with the Debye model for a solid, and the quadrupole shifts have been fit with a second order polynomial.

respectively; the latter magnetic component has a hyperfine field of of 2.31(5) T. The resulting fits, see the two green components in the 25 K spectrum shown in Figure 12, and the corresponding spectral parameters, see Table S3 (Supporting Information), are consistent with the electronic properties of $Nd_{18}Li_8Rh_3Fe_2O_{39}$.

The isomer shifts observed for $Nd_{18}Li_8Rh_3Fe_2O_{39}$ are compatible with the presence of low-spin iron(IV) on the 2*a* site and high-spin iron(III) on the 8*e* and 16*i* sites, spin- and oxidation states that are in agreement with those observed earlier[2] for $Nd_{18}Li_8Fe_5O_{39}$. Confidence in the model used for the Mössbauer spectral fits described above may be obtained through the temperature dependence of the isomer shifts, δ, and quadrupole splittings, ΔE_Q, observed for the 2*a*, 8*e*, and 16*i* sites, and their weighted average values, see Figure 13. As expected,[2] the three isomer shifts are essentially constant between 25 and 85 K and then decrease slightly upon further warming. The temperature dependencies of the isomer shifts of the 2*a*, 8*e*, and 16*i* sites and their weighted average, see the top of Figure 13, are well fit with the Debye model[8] for the second-order Doppler shift. The resulting Mössbauer temperatures, Θ_M, are 886(60), 565(100), 635(55), and 718(55) K, respectively.

The quadrupole splittings, ΔE_Q, observed for $Nd_{18}Li_8Rh_3Fe_2O_{39}$ are, as expected, almost independent of the temperature between 25 and 100 K and decrease slightly above 100 K. This very small change in ΔE_Q must arise from a small change in symmetry at each site with changing temperature. This small change is expected for high-spin iron(III) but is unexpected for low-spin iron(IV). Indeed, the change in ΔE_Q for the 2*a* site in $Nd_{18}Li_8Rh_3Fe_2O_{39}$ is much less than is observed above for $La_{18}Li_8Fe_5O_{39}$.

The temperature dependence of the logarithm of the Mössbauer spectral absorption area of $Nd_{18}Li_8Rh_3Fe_2O_{39}$ has been fit with the Debye model[8] for a solid, see the bottom of Figure 13, and yields a Debye temperature, Θ_D, of 430(18) K between 25 and 295 K, a value that is very similar to that of 438(12) K found in $La_{18}Li_8Fe_5O_{39}$.

Discussion

The results presented in Tables 1 and 6 and Figures 6 and 12 demonstrate that the substitution of iron into $Ln_{18}Li_8Rh_5O_{39}$ does not involve the random substitution of iron for rhodium over both the 2*a* and 8*e* sites. Instead, at low levels of substitution, a disproportionate amount of iron occupies the 2*a* site, with a smaller fraction going to the 8*e* site and an even smaller fraction to the 16*i* sites. In effect, the low-spin Rh(IV) which occupies the 2*a* site in the iron-free compositions[1,10] is replaced by low-spin iron(IV). This reduces the mean metal-to-oxygen bond length around the 2*a* site while the bond lengths around the 8*e* sites change relatively little (Tables 2 and 7). The La1−O distances in $La_{18}Li_8Rh_{5-x}Fe_xO_{39}$ are similar to those[1] in $La_{18}Li_8Rh_5O_{39}$, but the La2−O distances respond to the decrease in size of the 2*a* site. Comparing $x = 0$ and $x = 2.5$, the La2−O4 distance lengthens as the 2*a* site contracts, and the La2−O1 and La2−O3 distances contract in order to compensate. However, these two distances then increase as more iron is added to reach the composition $x = 3.5$, and the former shows a further increase (Table 4) when $x = 5$. The variation in the La2−O1 bond length thus follows the variation in the unit cell parameter shown in Figure 2. Unfortunately, the precision of our results is too low to show how the La2−O4 distance changes across the full composition range. The variation of the cell parameter at higher x values, where the 2*a* site is fully occupied by iron, might be attributable in part, to the increasing concentration of the relatively large Li^+ cation on the 8*e* site; this disorder was not observed in the iron-free composition. We do not have a full set of structural data for $Nd_{18}Li_8Rh_5O_{39}$, and our analysis of the Rh-rich end of the Nd-containing compositions thus lacks a reference point. However, the Nd2−O1 bond length is greater for $x = 5$[2] than for $x = 2$, consistent with the behavior of the La-containing system.

The composition dependence of the Curie constant for Ln = La is largely consistent with this account of the substitution process, although the discrepancy between the observed and calculated values is unusually large when $x = 3.5$. The Mössbauer spectral parameters determined at 295 K (Figure 8) are also in good agreement with the conclusions drawn from the diffraction data, although unusual behavior is again apparent for $x = 3.5$, this time in the composition dependence of the Mössbauer spectral absorption area expressed as (%ε)(mm/s)/(mg Fe/cm^2). For some at present unknown reason, for $x = 3.5$, and to a lesser extent for $x = 3$, the Mössbauer-effect recoil-free fraction is lower than expected.

The splitting of the t_{2g} orbitals (416(10) cm^{-1}) at the 2*a* site in $La_{18}Li_8Fe_5O_{39}$, signified by the temperature dependence of the quadrupole splitting, indicates that the cation site does not have cubic point symmetry. The observation of symmetry lowering by Mössbauer spectroscopy is consistent with the presence of disorder on the O4 site in the structural model. The temperature dependence of the Mössbauer isomer shift for this site in the compositions $x = 3.5$ and 4 is unusual (Table S2, Supporting Information); the value decreases significantly at low temperatures. The decrease begins at temperatures well above the point at which the gradient of $\chi(T)$ changes (cf. Figures 4 and 9). The explanation for this behavior is not obvious. One possible cause of a decrease in isomer shift is a high-spin to low-spin transition, but the 2*a* isomer shift for the composition $x = 3.5$ is consistent with the presence of low-spin Fe(IV) even at 295 K. Any change in the spin state of a cation should also be apparent in the magnetic susceptibility. Furthermore, in the composition $x = 3.5$, the decrease takes place over a wide temperature range, whereas spin-state crossovers in solids usually occur over a narrow temperature range. A change in the coordination geometry around the 2*a* site could also produce a marked change in the isomer shift. The isomer shifts associated with the 8*e* and 16*i* sites do not show anomalous behavior on cooling, and we can thus postulate that the thermal contraction of the structure that occurs on cooling is accommodated predominantly by a contraction of the bonds around the 2*a* site. Consideration of the data in Tables 2 and 4, together with those reported previously on related compounds,[2] shows that at room temperature the Fe−O4 bond length is longer in $La_{18}Li_8Rh_{1.5}Fe_{3.5}O_{39}$ than in comparable compounds, and that a relatively large contraction might therefore be possible on cooling. However, the weight that can be assigned to this evidence is severely restricted by the low precision associated with the bond lengths in Table 2. High-resolution structural studies of $La_{18}Li_8Rh_{1.5}Fe_{3.5}O_{39}$ would need to be carried out over a wide temperature range in order to confirm our hypothesis.

The Mössbauer spectral results on compositions having Ln = Nd are less extensive, but the spectral parameters (Figure 13) derived for $Nd_{18}Li_8Rh_3Fe_2O_{39}$ are consistent with the refined crystal structure described in Table 6. The temperature dependence of the isomer shift at the 2*a* site does not show the unusual temperature dependence found in some of the La-containing compositions. This is consistent with the observation of a relatively short Fe−O4 bond length (Table 7) at room temperature.

The magnetic behavior exhibited by members of this structural family is the result of interactions that might involve both d-block and f-block cations. This study is the first to undertake a direct comparison of two series based on the same transition metals (Rh, Fe) in the presence of one of two different lanthanides (La, Nd), the former being diamagnetic and the latter paramagnetic. Hence, we are able to make a direct assessment of the degree of involvement of the lanthanide cation in the magnetic interactions. Although the structural data discussed above demonstrate that both La and Nd can support a system of ⟨111⟩ channels that is able to accommodate polyhedral chains occupied by both Rh and Fe, comparison of Figures 4 and 10 shows that the low-temperature magnetic behaviors of the La- and Nd-containing compositions are very different. That of the latter resembles that observed in many Nd- or Pr-containing isostructural

compounds,[2−4] with the ac and dc susceptibility data (Figures 10 and 11) suggesting that a spin-glass-like phase is formed below 5 K in compositions having $x > 1$; the transition temperature increases with increasing Fe content. In contrast to that of $Nd_{18}Li_8Rh_3Fe_2O_{39}$, the magnetic susceptibility of $La_{18}Li_8Rh_3Fe_2O_{39}$ shows no maximum in the ZFC data. Both the ZFC and the FC susceptibilities continue to increase down to 2 K, although hysteresis is present below ∼8 K. The degree of hysteresis between the two curves increases with increasing iron content, but neither curve passes through a maximum for any composition. The difference in behavior of the two systems, Ln = La and Nd, which is emphasized further by a comparison of the ac susceptibility of $La_{18}Li_8Fe_5O_{39}$ (Figure 5) with that of $Nd_{18}Li_8Fe_5O_{39}$,[2] is strong evidence that the magnetic moment of the Ln cation plays a crucial role in the spin-freezing process in members of this structural family. This conclusion is also consistent with the low transition temperatures observed in all of the compositions studied to date.[2−4] The difference between the Ln = La and Nd compositions contrasts with the similarity between Ln = Nd and Pr compositions.[3,4] This supports the proposition that the differences stem from the variation in the magnetic properties of Ln rather than from the variation in ionic size. The nature of the transition in $La_{18}Li_8Fe_5O_{39}$, which was apparent in both the magnetometry and Mössbauer spectral data, remains unresolved. The neutron diffraction data and the Mössbauer spectra show that it does not correspond to the onset of long-range magnetic ordering, although the slow magnetic relaxation seen in the spectra suggests that long-range order could occur at still lower temperatures. Despite the absence of magnetic order, the ac susceptibility does not show the frequency dependence expected of a spin-glass, as it does in the case of $Nd_{18}Li_8Fe_5O_{39}$.

It is perhaps surprising that the transition-metal cations within the ⟨111⟩ polyhedral chains in all these compounds do not order magnetically at higher temperatures, particularly in view of the relatively high Néel temperatures shown by other compounds containing similar chains, for example, for Sr_3LiRuO_6, $T_N = 90$ K.[12] This can probably be ascribed to magnetic frustration among the interchain interactions within the $Ln_{18}Li_8Rh_{5-x}Fe_xO_{39}$ structure. The Mössbauer spectra do provide some evidence of the relative strengths of the exchange interactions experienced at the different sites. For example, that recorded from $Nd_{18}Li_8Rh_3Fe_2O_{39}$ at 25 K has an asymmetric magnetic component (Figure 12) associated with the 2*a* site, indicating that the spin relaxation slows at relatively high temperatures on this site compared to the 8*e* and 16*i* sites. However, the spectrum recorded from the relatively iron-rich composition $La_{18}Li_8Rh_{1.5}Fe_{3.5}O_{39}$ could be fitted without a magnetic component, further evidence that the Ln cation plays an important part in the magnetic coupling.

(12) Darriet, J.; Grasset, F.; Battle, P. D. *Mater. Res. Bull.* **1997**, *32*, 139.

Conclusion

The results described above demonstrate that, when iron is introduced into $Ln_{18}Li_8Rh_5O_{39}$, it preferentially occupies the 2*a* site, the smallest available, as low-spin iron(IV). The nonlinear dependence of the unit-cell parameter on the iron content reflects this nonrandom substitution. Increasing the concentration of iron in $Ln_{18}Li_8Rh_{5-x}Fe_xO_{39}$ leads to a departure from the paramagnetic behavior seen in the $x = 0$ compositions. However, for Ln = La or Nd, no ground state showing long-range magnetic order is observed above 3 K. Below ∼5 K, compositions with $x > 1$ containing Nd, but not those containing La, show behavior which is characteristic of a spin-glass. The La-containing compositions show irreversible magnetic behavior below ∼8 K, but the nature of the ground state remains undetermined.

Acknowledgment. We are grateful to Dr. C. Ritter for providing experimental assistance at the ILL in Grenoble, France. Exploratory experimental work was undertaken in Oxford by F. Freestone. F.G. acknowledges the financial support of the Fonds National de la Recherche Scientifique, grants 9.456595 and 1.5.064.05. N.T. is supported by a Royal Thai Government Scholarship.

Supporting Information Available: Additional supporting information is provided in PDF format for the Mössbauer spectral fits. This material is available free of charge via the Internet at http://pubs.acs.org.